Structure and Function of Nucleoside Hydrolases from *Physcomitrella patens* and Maize Catalyzing the Hydrolysis of Purine, Pyrimidine, and Cytokinin Ribosides[1][W]

Martina Kopečná, Hanna Blaschke, David Kopečný*, Armelle Vigouroux, Radka Končitíková, Ondřej Novák, Ondřej Kotland, Miroslav Strnad, Solange Moréra*, and Klaus von Schwartzenberg*

Department of Protein Biochemistry and Proteomics, Center of the Region Haná for Biotechnological and Agricultural Research (M.K., D.K., R.K.), Department of Biochemistry (R.K., O.K.), Faculty of Science, Palacký University, CZ–783 71 Olomouc, Czech Republic; Laboratory of Growth Regulators, Palacký University and Institute of Experimental Botany, Academy of Sciences of the Czech Republic, CZ–783 71 Olomouc, Czech Republic (O.N., O.K., M.S.); Biozentrum Klein Flottbek und Botanischer Garten, Universität Hamburg, D–22609 Hamburg, Germany (H.B., K.v.S.); and Laboratoire d'Enzymologie et Biochimie Structurales, CNRS, F–91198 Gif-sur-Yvette cedex, France (A.V., S.M.)

We present a comprehensive characterization of the nucleoside *N*-ribohydrolase (NRH) family in two model plants, *Physcomitrella patens* (PpNRH) and maize (*Zea mays*; ZmNRH), using in vitro and in planta approaches. We identified two NRH subclasses in the plant kingdom; one preferentially targets the purine ribosides inosine and xanthosine, while the other is more active toward uridine and xanthosine. Both subclasses can hydrolyze plant hormones such as cytokinin ribosides. We also solved the crystal structures of two purine NRHs, PpNRH1 and ZmNRH3. Structural analyses, site-directed mutagenesis experiments, and phylogenetic studies were conducted to identify the residues responsible for the observed differences in substrate specificity between the NRH isoforms. The presence of a tyrosine at position 249 (PpNRH1 numbering) confers high hydrolase activity for purine ribosides, while an aspartate residue in this position confers high activity for uridine. Bud formation is delayed by knocking out single NRH genes in *P. patens*, and under conditions of nitrogen shortage, PpNRH1-deficient plants cannot salvage adenosine-bound nitrogen. All PpNRH knockout plants display elevated levels of certain purine and pyrimidine ribosides and cytokinins that reflect the substrate preferences of the knocked out enzymes. NRH enzymes thus have functions in cytokinin conversion and activation as well as in purine and pyrimidine metabolism.

Nucleoside hydrolases or nucleoside *N*-ribohydrolases (NRHs; EC 3.2.2.-) are glycosidases that catalyze the cleavage of the *N*-glycosidic bond in nucleosides to enable the recycling of the nucleobases and Rib (Fig. 1A). The process by which nucleosides and nucleobases are recycled is also known as salvaging and is a way of conserving energy, which would otherwise be needed for the de novo synthesis of purine- and pyrimidine-containing compounds. During the salvage, bases and nucleosides can be converted into nucleoside monophosphates by the action of phosphoribosyltransferases and nucleoside kinases, respectively, and further phosphorylated into nucleoside diphosphates and triphosphates (Moffatt et al., 2002; Zrenner et al., 2006; Fig. 1B). Uridine kinase and uracil phosphoribosyl transferase are key enzymes in the pyrimidine-salvaging pathway in plants (Mainguet et al., 2009; Chen and Thelen, 2011). Adenine phosphoribosyltransferase and adenosine kinase (ADK) are important in purine salvaging (Moffatt and Somerville, 1988; Moffatt et al., 2002), and their mutants cause reductions in fertility or sterility, changes in transmethylation, and the formation of abnormal cell walls. In addition, both enzymes were also reported to play roles in cytokinin metabolism (Moffatt et al., 1991, 2000; von Schwartzenberg et al., 1998; Schoor et al., 2011). Cytokinins (N^6-substituted adenine derivatives) are plant hormones that regulate

[1] This work was supported by the Czech Science Foundation (grant no. P501/11/1591), the Ministry of Education, Youth, and Sports of the Czech Republic (grant no. MSM 6198959215), Palacký University (grant no. PrF_2013_037), Operational Programme Research and Development for Innovation (grant no. ED0007/01/01), the Centre National de la Recherche Scientifique (to S.M. and A.V.), the Deutsch Forschungsgemeinschaft (grant no. SCHW687/6 to K.v.S. and H.B.), and the Appuhn Foundation (Hamburg). M.K. was a Federation of European Microbiological Societies fellow.

* Address correspondence to david.kopecny@upol.cz, morera@lebs.cnrs-gif.fr, and klaus.von.schwartzenberg@uni-hamburg.de.

The author responsible for distribution of materials integral to the findings presented in this article in accordance with the policy described in the Instructions for Authors (www.plantphysiol.org) is: David Kopečný (david.kopecny@upol.cz).

D.K., S.M., and K.v.S. designed the research; M.T., H.B., D.K., and R.K. analyzed enzyme kinetics; A.V. and S.M. performed the crystallographic study and contributed material and tools for crystallography; S.M. and D.K. analyzed the crystal structures; H.B. and K.v.S. generated and analyzed *P. patens* mutants, and O.N., O.K., and M.S. analyzed the metabolite levels. D.K., S.M., and K.v.S. wrote the paper.

[W] The online version of this article contains Web-only data.
www.plantphysiol.org/cgi/doi/10.1104/pp.113.228775

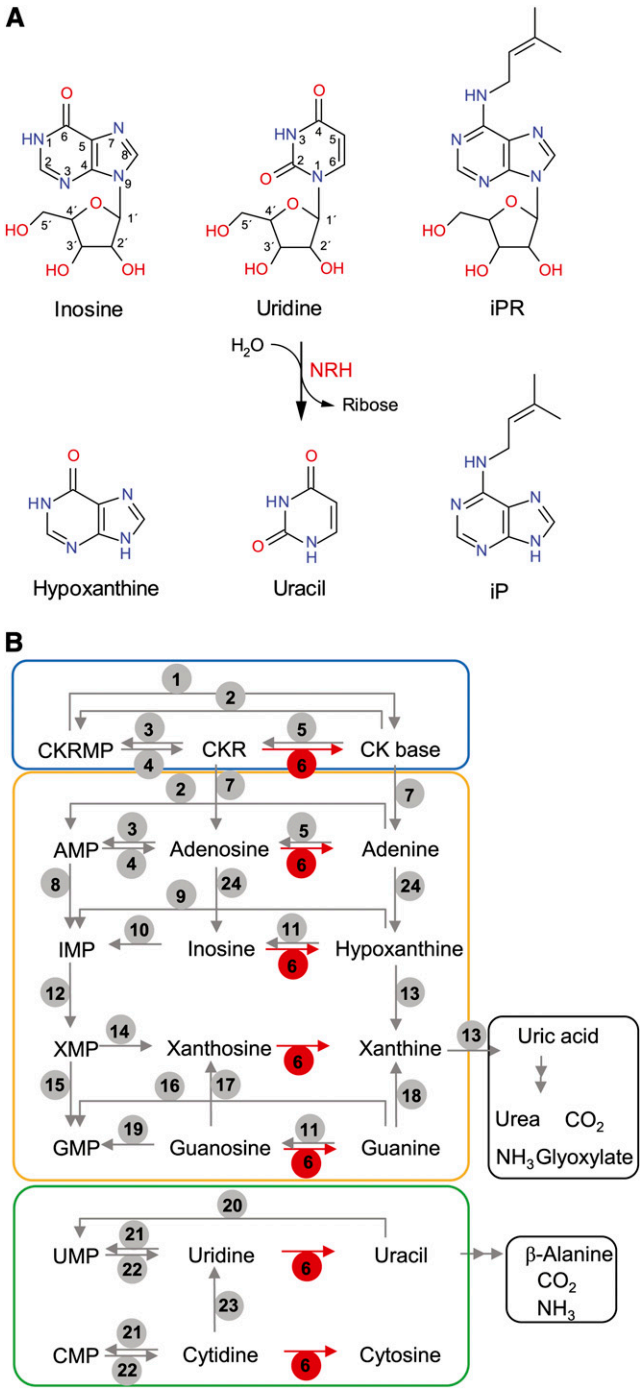

Figure 1. A, Scheme of the reactions catalyzed by plant NRHs when using purine (inosine), pyrimidine (uridine), and cytokinin (iPR) ribosides as the substrates. B, Simplified schematic overview of cytokinin, purine, and pyrimidine metabolism in plants. The diagram is adapted from the work of Stasolla et al. (2003) and Zrenner et al. (2006) with modifications. The metabolic components shown are as follows: 1, cytokinin nucleotide phosphoribohydrolase; 2, adenine phosphoribosyltransferase; 3, adenosine kinase; 4, 5′-nucleotidase; 5, adenosine phosphorylase; 6, purine/pyrimidine nucleoside ribohydrolase; 7, cytokinin oxidase/dehydrogenase; 8, AMP deaminase; 9, hypoxanthine phosphoribosyltransferase; 10, inosine kinase; 11, inosine-guanosine phosphorylase; 12, IMP dehydrogenase; 13, xanthine dehydrogenase; 14, 5′-nucleotidase; 15, GMP synthase; 16, hypoxanthine-guanine phosphoribosyltransferase; 17, guanosine deaminase; 18, guanine deaminase; 19, guanosine kinase; 20, uracil phosphoribosyltransferase; 21, uridine cytidine kinase; 22, pyrimidine 5′-nucleotidase; 23, cytidine deaminase; 24, adenosine/adenine deaminase. CK, Cytokinin; CKR, cytokinin riboside; CKRMP, cytokinin riboside monophosphate.

cell division and numerous developmental events (Mok and Mok, 2001; Sakakibara, 2006). Cytokinin ribosides are considered to be transport forms and have little or no activity.

NRHs are metalloproteins first identified and characterized in parasitic protozoa such as *Trypanosoma*, *Crithidia*, and *Leishmania* species that rely on the import and salvage of nucleotide derivatives. They have since been characterized in other organisms such as bacteria, yeast, and insects (Versées and Steyaert, 2003) but never in mammals (Parkin et al., 1991). They have been divided into four classes based on their substrate specificity: nonspecific NRHs, which hydrolyze inosine and uridine (IU-NRHs; Parkin et al., 1991; Shi et al., 1999); purine-specific inosine/adenosine/guanosine NRHs (Parkin, 1996); the 6-oxopurine-specific guanosine/inosine NRHs (Estupiñán and Schramm, 1994); and the pyrimidine nucleoside-specific cytidine/uridine NRHs (CU-NRHs; Giabbai and Degano, 2004). All NRHs exhibit a stringent specificity for the Rib moiety and differ in their preferences regarding the nature of the nucleobase. Crystal structures are available for empty NRH or in complex with inhibitors from *Crithidia fasciculata* (CfNRH; Degano et al., 1998), *Leishmania major* (LmNRH; Shi et al., 1999), and *Trypanosoma vivax* (TvNRH; Versées et al., 2001, 2002). The structures of two CU-NRHs from *Escherichia coli*, namely YeiK (Iovane et al., 2008) and YbeK (rihA; Muzzolini et al., 2006; Garau et al., 2010), are also available. NRHs are believed to catalyze *N*-glycosidic bond cleavage by a direct displacement mechanism. An Asp from a conserved motif acts as a general base and abstracts a proton from a catalytic water molecule, which then attacks the C1′ atom of the Rib moiety of the nucleoside. Kinetic isotope-effect studies on CfNRH (Horenstein et al., 1991) showed that the substrate's hydrolysis proceeds via an oxocarbenium ion-like transition state and is preceded by protonation at the N7 atom of the purine ring, which lowers the electron density on the purine ring and destabilizes the *N*-glycosidic bond. A conserved active-site His is a likely candidate for this role in IU-NRHs and CU-NRHs. In the transition state, the C1′-N9 glycosidic bond is almost 2 Å long, with the C1′ atom being sp^2 hybridized while the C3′ atom adopts an exo-conformation, and the whole ribosyl moiety carries a substantial positive charge (Horenstein et al., 1991).

Several NRH enzymes have been identified in plants, including a uridine-specific NRH from mung bean (*Phaseolus radiatus*; Achar and Vaidyanathan, 1967), an inosine-specific NRH (EC 3.2.2.2) and a guanosine-inosine-specific NRH, both from yellow lupine (*Lupinus luteus*; Guranowski, 1982; Szuwart et al., 2006), and an adenosine-specific NRH (EC 3.2.2.7) from coffee

(*Coffea arabica*), barley (*Hordeum vulgare*), and wheat (*Triticum aestivum*; Guranowski and Schneider, 1977; Chen and Kristopeit, 1981; Campos et al., 2005). However, their amino acid sequences have not been reported so far. A detailed study of the *NRH* gene family from Arabidopsis (*Arabidopsis thaliana*) has recently been reported (Jung et al., 2009, 2011). The AtNRH1 enzyme exhibits highest hydrolase activity toward uridine and xanthosine. It can also hydrolyze the cytokinin riboside N^6-(2-isopentenyl)adenosine (iPR), which suggests that it may also play a role in cytokinin homeostasis. However, Riegler et al. (2011) analyzed the phenotypes of homozygous *nrh1* and *nrh2* single mutants along with the homozygous double mutants and concluded that AtNRHs are probably unimportant in cytokinin metabolism.

Here, we identify and characterize plant IU-NRHs from two different model organisms, *Physcomitrella patens* and maize (*Zea mays*), combining structural, enzymatic, and in planta functional approaches. The moss *P. patens* was chosen to represent the bryophytes, which can be regarded as being evolutionarily basal terrestrial plants, and is suitable for use in developmental and metabolic studies (Cove et al., 2006; von Schwartzenberg, 2009), while maize is an important model system for cereal crops. We report the crystal structures of NRH enzymes from the two plant species, PpNRH1 and ZmNRH3. Based on these structures, we performed site-directed mutagenesis experiments and kinetic analyses of point mutants of PpNRH1 in order to identify key residues involved in nucleobase interactions and catalysis. To analyze the physiological role of the PpNRHs, single knockout mutants were generated. NRH deficiency caused significant changes in the levels of purine, pyrimidine, and cytokinin metabolites relative to those seen in the wild type, illustrating the importance of these enzymes in nucleoside and cytokinin metabolism.

RESULTS AND DISCUSSION

Gene Models of NRHs from *P. patens* and Maize

Ongoing genomic analyses suggest that most plant genomes contain at least two genes coding for NRHs. Several plant genomes, such as those of moss (*P. patens*), maize, Arabidopsis, rice (*Oryza sativa*), tomato (*Solanum lycopersicum*), and wheat, appear to contain several *NRHs*. We focused on two model plant organisms, the moss *P. patens* and maize, due to the availability of detailed information on cytokinin metabolism in both species (Massonneau et al., 2004; von Schwartzenberg, 2009; Vyroubalová et al., 2009). The genome databases for the moss *P. patens* (www.phytozome.net, version 9.1) and maize (www.maizesequence.org, version 5b.60) indicate that these species contain three and five *NRH* genes, respectively. In order to identify the correct gene models in each case and obtain the corresponding recombinant proteins, we cloned the complementary DNAs (cDNAs) of these eight *NRHs* using gene-specific primers and deposited their sequences to GenBank (see "Materials and Methods").

The cDNA sequence obtained for *PpNRH1* corresponds to the predicted gene model (Pp1s357_22V6.1), those obtained for *PpNRH2* and *PpNRH3* do not match the predicted gene models in the genome annotation version 6.1 (Pp1s140_172V6.1 and Pp1s5_276V6.1; see "Materials and Methods"; Supplemental Fig. S1). The two paralogous genes *ZmNRH1a* and *ZmNRH1b* are localized on chromosomes 8 and 3 (GRMZM2G029845 and GRMZM2G134149), respectively. The two other paralogs, *ZmNRH2a* and *ZmNRH2b*, lie on chromosomes 4 and 1 (GRMZM2G085960 and GRMZM2G015344), respectively. The last *ZmNRH3* gene (GRMZM2G104999) is localized on chromosome 2. These genes encode proteins of between 315 and 341 residues. All plant NRHs exhibit a conserved sequence motif, DTDPGIDD, at the N terminus (Fig. 2), which is involved in the binding of a calcium ion and the Rib moiety of the substrate (Versées and Steyaert, 2003). Another group of extracellular NRHs with two domains was recently identified in Arabidopsis (At5g18860; Jung et al., 2011). The authors suggested that these NRHs could correspond with the extracellular adenosine hydrolase activity found in potato (*Solanum tuberosum*) tubers (Riewe et al., 2008). Although the first domain carries a DTDVDTDD motif, the second contains an unconserved DMDMSXGD motif. Analogous sequences are also present in the genomes of other

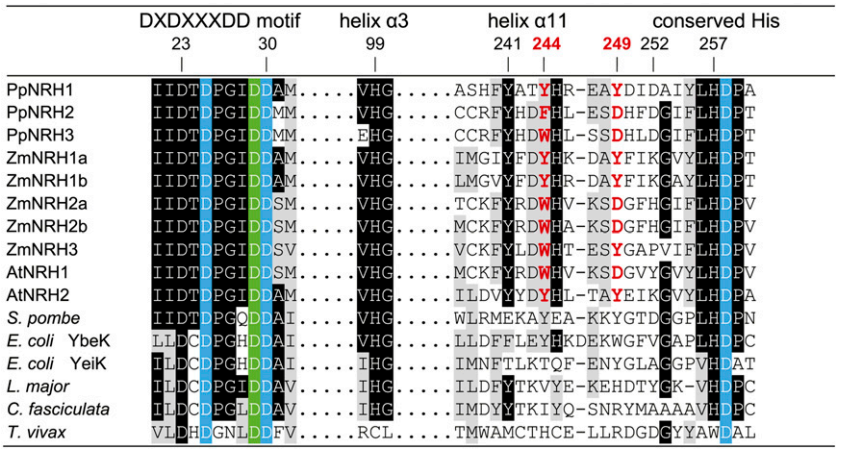

Figure 2. Multiple alignment of the amino acid sequences of NRHs from plants, yeast, bacteria, and protozoa, focusing on the DXDXXXDD motif and the α3 and α11 helix regions. Asp residues involved in calcium ion coordination are highlighted in blue. The Asp-binding 2-OH group of Rib is highlighted in green. Crucial residues involved in substrate binding in plant NRHs are highlighted in red. Residues are numbered according to the PpNRH1 sequence. Accession numbers for the sequences shown are listed in "Materials and Methods."

plants such as maize (GRMZM2G386229) and rice (Os05g33644 and Os05g33630).

Substrate Specificity of Plant NRHs

The pH effect on the specific activity of PpNRH1 (Supplemental Fig. S2) was analyzed, and high activity was found between pH 7.0 and 9.0. All subsequent kinetic analyses, therefore, were performed at pH 7.5. PpNRH1, ZmNRH2a, ZmNRH2b, and ZmNRH3 were obtained active and in high yield in soluble form. In contrast, the production of PpNRH2, ZmNRH1a, and ZmNRH1b primarily resulted in the formation of inclusion bodies, and refolding attempts did not lead to restoration of the enzymatic activity. Only very small quantities of these enzymes could be obtained in soluble form. We thus were only able to briefly screen the three NRHs with possible natural substrates, including purine, pyrimidine, and cytokinin ribosides, at 200 μM concentration (Table I). It was possible to analyze the substrate preferences for PpNRH2, whereas ZmNRH1a and ZmNRH1b show only negligible activity. However, cytidine and adenosine could be substrates of the two maize enzymes, but we cannot rule out that untested ribosides can be more suitable substrates. So far, the production of recombinant protein was not observed for any of the four splicing variants of PpNRH3, in contrast to the studied NRHs.

PpNRH1 is most active toward the two purine ribosides xanthosine and inosine and exhibits weaker activity with adenosine, uridine, and guanosine. In contrast, PpNRH2 prefers the pyrimidine riboside uridine and is less active toward xanthosine and inosine. ZmNRH2a and ZmNRH2b are also most active toward uridine. The activity of ZmNRH2b is 10 and 200 times higher than that of ZmNRH2a and PpNRH2, respectively. The comparatively low activity of PpNRH2 is likely due to being poorly expressed in *E. coli* and its low stability. ZmNRH3 preferentially hydrolyzes inosine and xanthosine, while the remaining nucleosides are weaker substrates. PpNRH1 and ZmNRH3 exhibit similar substrate preferences. However, subtle differences between these two enzymes are shown in Figure 3.

PpNRH1, ZmNRH2a, ZmNRH2b, and ZmNRH3 were further analyzed to determine their K_m and catalytic constant (k_{cat}) values (Table II) and confirmed the results discussed above. Both PpNRH1 and ZmNRH3 show the highest catalytic efficiency with inosine and xanthosine, while ZmNRH2a and ZmNRH2b display the highest catalytic efficiency for uridine and xanthosine. Although ZmNRH2a and ZmNRH2b have relatively high K_m values for uridine, it is also the substrate for which they have the highest k_{cat} values. Based on these kinetic values and the current system of classification, the investigated plant NRHs belong to the nonspecific IU-NRH class (Parkin et al., 1991; Shi et al., 1999). However, both PpNRH1 and ZmNRH3 (which prefer inosine and xanthosine) are apparently kinetically different from ZmNRH2a, ZmNRH2b, and PpNRH2 (all of which prefer uridine and xanthosine) and the AtNRH1 from Arabidopsis (Jung et al., 2009, 2011). Therefore, it seems that there are at least two subclasses of IU-NRHs in plants. Details of the sequences of these two subclasses are discussed below.

Inosine, xanthosine, and guanosine are all intermediates in the purine catabolic pathway (Fig. 1B) that starts with AMP (Zrenner et al., 2006). The xanthine and hypoxanthine nucleobases are formed by the action of nucleoside hydrolases and are further processed by xanthine dehydrogenase to give uric acid. Adenosine and adenine are by-products of the cytokinin degradation reactions catalyzed by cytokinin oxidase/dehydrogenase (EC 1.5.99.12; Houba-Hérin et al., 1999). In contrast to the two known bacterial CU-NRHs, the five plant IU-NRHs exhibit very weak activity toward cytidine (Table I). This is consistent with the fact that plants preferentially convert cytidine to uridine via cytidine deaminase (EC 3.5.4.5; Stasolla et al., 2003). To analyze the conversion of cytokinin ribosides, we first determined the extinction coefficients of iPR and trans-zeatin riboside (tZR) by spectrometric measurement according to Parkin (1996). All of the studied plant IU-NRHs have only weak activity toward iPR and tZR, between 1% and 0.1% of that toward their best substrates (Table I). ZmNRH2b and ZmNRH3 exhibit catalytic efficiencies between 1.7 and 5.3 $\times$ 10^2 M^{-1} s^{-1} (Table II). The

Table I. *Substrate specificity of NRHs from P. patens and maize*

Relative reaction rates (%) were measured at 200 μM substrate concentration. Activities were measured in 200 mM Tris-HCl buffer (pH 7.5) containing 400 mM KCl and 1 mM DTT. The specific activities for PpNRH1 and ZmNRH3 with 200 μM xanthosine were 135 and 61 nkat mg^{-1}, respectively. The specific activities for PpNRH2, ZmNRH2a, and ZmNRH2b with 200 μM uridine were 1.3, 26, and 226 nkat mg^{-1}, respectively. + indicates very low activity.

Substrate	Relative Rate				
	PpNRH1	PpNRH2	ZmNRH2a	ZmNRH2b	ZmNRH3
Inosine	87	22	9.3	9.5	100
Xanthosine	100	61	53	34	70
Adenosine	6.1	1.6	15	3.5	2
Guanosine	1.7	0	0.1	0.5	1.5
Uridine	5.7	100	100	100	5
Cytidine	0.1	3.9	5.0	0.9	0.1
iPR	0.1	+	0.03	0.3	1.4
tZR	0.1	+	0.03	0.3	1.5

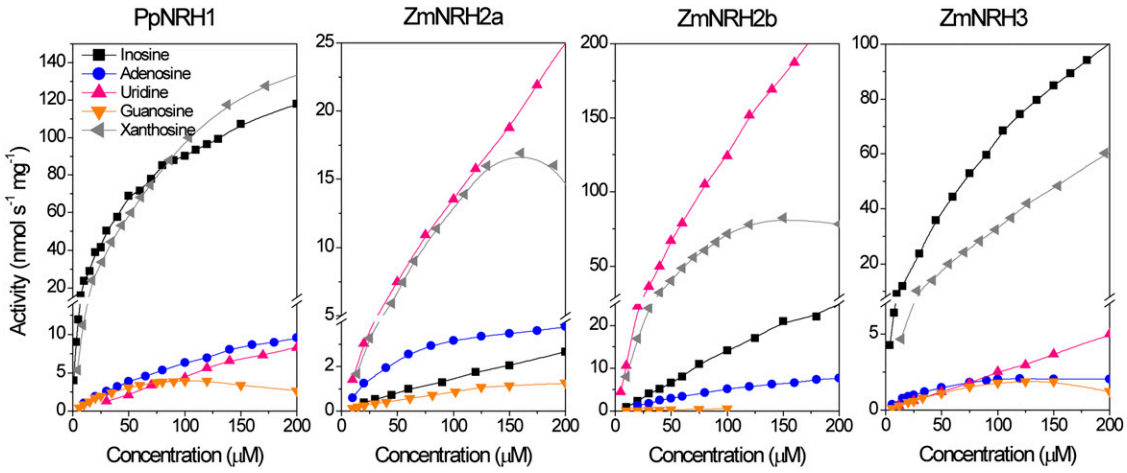

Figure 3. Saturation curves of activity for PpNRH1, ZmNRH2a, ZmNRH2b, and ZmNRH3. Data were measured with five substrates (inosine, xanthosine, adenosine, guanosine, and uridine) in 200 mM Tris-HCl buffer (pH 7.5) containing 400 mM KCl and 2 mM DTT.

conversion of the substrates by PpNRH1 and PpNRH2 was further confirmed by HPLC analysis using tritiated iPR and by HPLC-UV analysis for PpNRH1, ZmNRH2b, and ZmNRH3 (Supplemental Fig. S3).

Crystal Structure and Substrate Binding in Plant NRHs

The crystal structures of PpNRH1 and ZmNRH3 are, to our knowledge, the first reported crystal structures for any plant NRH. The asymmetric unit of the PpNRH1 crystal contains four very similar dimers with an average root mean square deviation (RMSD) of 0.75 Å for all Cα atoms. The asymmetric unit of the ZmNRH3 crystal contains only one dimer (Fig. 4A; Supplemental Table S1). This is consistent with the results from gel filtration chromatography showing that the active form in solution is a dimer (Supplemental Fig. S4). PpNRH1 and ZmNRH3 monomers and dimers are very similar to each other, with average RMSD values of 0.9 and 1.2 Å for all Cα atoms, respectively. Each monomer possesses a typical NRH fold containing 12 β-strands and 13 α-helices. Indeed, a structural comparison of the plant NRH monomer with all entries in the Protein Data Bank (PDB) using Secondary Structure Matching-program (European Bioinformatics Institute) revealed that it resembles numerous NRH structures from protozoa and bacteria, such as TvNRH, CfNRH, LmNRH, YeiK, and YbeK, with RMSD values ranging from 1.4 to 1.8 Å over 283 to 338 Cα atoms, corresponding to a sequence identity of 31% to 34% (Supplemental Fig. S5). The major structural difference concerns the loop region 278 to 294 (PpNRH1 numbering) involved in dimer contact, which is longer in plant NRHs than in all other known NRHs. All of the NRHs studied to date are homotetramers, except for TvNRH, which is a homodimer (Versées et al., 2001). Although PpNRH1 and ZmNRH3 are dimeric, their dimer is different from that of TvNRH. The ZmNRH3 and PpNRH1 dimer interfaces, which cover 1,262 and 1,278 Å^2 per subunit, respectively, involve three regions (residues 156–164, 228–223, and 263–289) that form hydrophobic interactions and are complemented by 10 hydrogen bonds.

A conserved Ca^{2+} ion in the active site is tightly bound to the Asp-25, Asp-30, and Asp-258 (Asp-8, Asp-13, and Asp-240) and to the main-chain carbonyl group of Leu-141 (Leu-123) in PpNRH1 (ZmNRH3 numbering). Its octahedral coordination can be completed either by three water molecules or by a catalytic

Table II. *Kinetic parameters for PpNRH1, ZmNRH2a, ZmNRH2b, and ZmNRH3*

Activities were measured in 200 mM Tris-HCl buffer (pH 7.5) containing 400 mM KCl and 1 mM DTT and using substrates up to 600 μM concentration. Kinetic constants were determined with GraphPad Prism 5.0 data-analysis software. –, Not determined.

Substrate	PpNRH1			ZmNRH2a			ZmNRH2b			ZmNRH3		
	K_m	k_{cat}	k_{cat}/K_m	K_m	k_{cat}	k_{cat}/K_m	K_m	k_{cat}	k_{cat}/K_m	K_m	k_{cat}	k_{cat}/K_m
	μM	s^{-1}	$s^{-1}\ M^{-1}$	μM	s^{-1}	$s^{-1}\ M^{-1}$	μM	s^{-1}	$s^{-1}\ M^{-1}$	μM	s^{-1}	$s^{-1}\ M^{-1}$
Inosine	78 ± 5	6.0 ± 0.3	7.7×10^4	1,013 ± 115	0.61 ± 0.05	6.0×10^2	713 ± 62	4.1 ± 0.3	5.7×10^3	201 ± 7	7.2 ± 0.2	3.6×10^4
Xanthosine	116 ± 9	7.0 ± 0.4	6.1×10^4	178 ± 28	1.3 ± 0.25	7.5×10^3	109 ± 19	4.6 ± 0.6	4.2×10^4	396 ± 50	6.2 ± 0.7	1.6×10^4
Adenosine	113 ± 7	0.6 ± 0.03	5.4×10^3	60 ± 4	0.18 ± 0.03	3.0×10^3	111 ± 17	0.4 ± 0.03	3.5×10^3	39 ± 4	0.12 ± 0.01	3.0×10^3
Guanosine	61 ± 6	0.2 ± 0.01	3.5×10^3	121 ± 14	0.07 ± 0.01	5.7×10^2	60 ± 13	0.03 ± 0.01	3.9×10^2	104 ± 18	0.12 ± 0.01	1.2×10^3
Uridine	890 ± 102	1.4 ± 0.2	1.5×10^3	468 ± 66	3.0 ± 0.24	6.4×10^3	514 ± 41	23.8 ± 1.5	4.6×10^4	1030 ± 180	1.1 ± 0.1	1.1×10^3
iPR	–	–	–	–	–	–	402 ± 53	0.07 ± 0.01	1.8×10^2	196 ± 20	0.10 ± 0.01	5.3×10^2
tZR	–	–	–	–	–	–	412 ± 36	0.07 ± 0.01	1.7×10^2	428 ± 48	0.17 ± 0.01	4.0×10^2

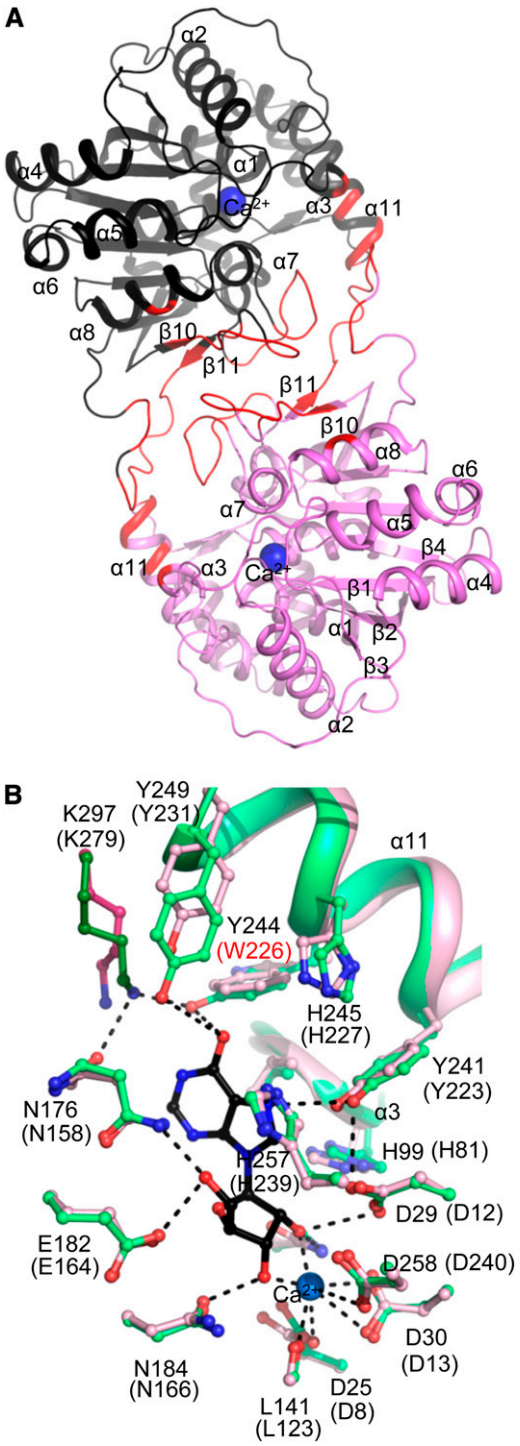

Figure 4. Crystal structure of plant NRHs. A, Dimeric structure of PpNRH1. One subunit is colored in black and the other in violet. The calcium ion in the active site is shown as a blue sphere. Intersubunit contacts are shown in red. B, Substrate-binding sites of PpNRH1 (in green) and ZmNRH3 (in pink). A molecule of inosine (in black) was docked into the active site. Amino acid residues are labeled and H-bonds, and calcium ion coordination are shown as dashed lines. Differences in the sequences of the two NRHs are labeled in red.

water molecule and the 2′- and 3′-hydroxyl groups of the substrate Rib moiety. The catalytic water molecule in turn interacts with the catalytic base, which is believed to increase the nucleophilicity of the water molecule attacking the C1′-N9 bond of the substrate. The calcium ion is believed to lower the pK_a of the catalytic water molecule prior to proton transfer to the active site base (Degano et al., 1998). Based on the sequence similarity and structural comparisons with protozoan NRHs (Versées et al., 2001), we designed and produced D25A and D8A mutants of PpNRH1 and ZmNRH3, respectively, to verify the roles of the targeted Asp residues as catalytic bases. Both mutants exhibit 10^4-fold lower activity than the wild-type proteins (Table III). These results confirm that the second Asp of the DTDPGIDD conserved motif functions as the active site base in plant NRHs. A similar result was reported for the equivalent D10A mutant in TvNRH (Versées et al., 2002), which was between 10^3 and 10^4 times less active than the wild-type enzyme but has an identical K_m value.

Soaking or cocrystallization of WT-PpNRH1 and D25A-PpNRH1, as well as of WT-ZmNRH3 and D8A-ZmNRH3, with nucleosides or inhibitors was unsuccessful. Therefore, we resorted to modeling and docking studies to understand the determinants for the substrate specificities of plant NRHs. We used the structure of YeiK in complex with inosine (PDB 3B9X) to model a substrate into the active sites of PpNRH1 and ZmNRH3 by structural superposition. The Rib moiety is tightly bound to conserved residues among the NRH family corresponding to Asn-176, Glu-182, Asp-258, Asn-184, Asp-29, Asp-30, and Asn-54 in PpNRH1 (Asn-158, Glu-164, Asp-240, Asn-166, Asp-12, Asp-13, and Asn-37 in ZmNRH3). In contrast, the nucleobase is surrounded by more variable residues (PpNRH1 numbering): Val-98 and His-99 from helix α3; aromatic residues Tyr-241, Tyr-244, His-245, and Tyr-249 from helix α11; His-257 in helix α12; Asn-176 in the β5-α7 loop; the adjacent side chain of Lys-297, which protrudes into the active site from the other subunit and is hydrogen bonded to Tyr-244; and the main-chain oxygen of Asn-176. A structural comparison of the substrate-binding sites of PpNRH1 and ZmNRH3 (Fig. 4B) shows that only one residue is different around the nucleobase, Tyr-244 in PpNRH1 is replaced by a Trp in ZmNRH3.

IU-NRHs such as CfNRH (Parkin et al., 1991; Degano et al., 1996) are characterized by a catalytic triad that consists of one His and two Tyr residues. These residues belong to a particular α9 helix (equivalent to the α11 helix in plant NRHs) that is known to move upon substrate binding in CU-NRHs from *E. coli* (Giabbai and Degano, 2004; Muzzolini et al., 2006; Iovane et al., 2008; Garau et al., 2010). This triad binds the substrate and allows the efficient protonation of the N7 atom of the purine base (the leaving group). Intriguingly, no such triad is present in the CU-NRHs, suggesting that the residues required for leaving group activation when protonating pyrimidine bases are different from those required for purines. In CfNRH, the triad consists of Tyr-229, Tyr-225, and His-241; His-241 is the residue

Table III. *Kinetic parameters for PpNRH1 and mutant proteins with the potential natural substrates inosine and xanthosine*

Relative reaction rates (%) were measured at 200 μM substrate concentration in 200 mM Tris-HCl buffer (pH 7.5) containing 400 mM KCl and 1 mM DTT. The concentration was chosen to avoid a substrate inhibition effect as observed with xanthosine. Kinetic constants K_m and k_{cat} were determined using GraphPad Prism 5.0 software. n.d., Not determined due to negligible activity.

Enzyme	Relative Rate Inosine/Xanthosine	Inosine			Xanthosine		
		K_m	k_{cat}	k_{cat}/K_m	K_m	k_{cat}	k_{cat}/K_m
	%	μM	s^{-1}	$s^{-1}\ M^{-1}$	μM	s^{-1}	$s^{-1}\ M^{-1}$
WT-PpNRH1	100/115	78	6.0	7.7×10^4	116	7.0	6.1×10^4
D25A	100/106	n.d.	5.4×10^{-4}	n.d.	n.d.	5.8×10^{-4}	n.d.
H99A	n.d.	n.d.	n.d.	n.d.	n.d.	n.d.	n.d.
Y241A	100/340	630	0.06	1.0×10^2	487	0.19	4.0×10^2
Y244A	100/188	1,208	1.4	1.2×10^3	206	0.58	2.8×10^3
H245A	100/240	1,090	1.1	1.0×10^3	356	1.3	3.6×10^3
E247A	100/124	94	5.7	6.1×10^4	140	7.2	5.1×10^4
Y249A	100/270	1,390	0.7	5.2×10^2	596	1.1	1.8×10^3
D250A	100/108	134	7.2	5.3×10^4	171	8.4	4.9×10^4
D252A	100/115	301	3.0	1.0×10^4	232	2.5	1.1×10^4
Y255A	100/190	760	0.47	6.2×10^2	367	0.43	1.2×10^3

that protonates the N7 atom (Fig. 5A; Gopaul et al., 1996). PpNRH1, which is an IU-NRH, possesses an equivalent triad consisting of His-245, Tyr-241, and His-257, in which His-257 is expected to protonate the leaving group. However, in this work, we mutated His-99 into Ala in PpNRH1 and found this mutant inactive with any riboside tested as a substrate. His-99 is conserved in all NRHs except for TvNRH. In our docking experiments (see below), His-99 is only 3.2 to 3.5 Å away from the N9 atom of the purine ring as well as the N1 and O2 atoms of a docked pyrimidine ring, indicating that it is another potential proton donor. Interestingly, Giabbai and Degano (2004) concluded from their mutagenesis analysis on two potential catalytic acids in bacterial YeiK (His-82 and His-239, equivalent to His-99 and His-257 in PpNRH1) that other active-site residues can function as alternative proton donors that could contribute to the *N*-glycosidic bond cleavage in this CU-NRH. The PpNRH1 substrate-binding site involves two additional residues, Tyr-244 and Tyr-249, which point toward the nucleobase compared with their equivalent residues Ile-228 and Tyr-234 in CfNRH. In CfNRH, the substrate-binding site is completed by the Arg-233 residue, which is located in the loop following the mobile α9 helix. Interestingly, the side chain of Lys-297 (from the neighboring subunit in PpNRH1) occupies a position similar to that of Arg-233 (Fig. 5A), suggesting that the dimer formation has an important role in enzymatic function of plant NRHs.

Docking Analysis and Site-Directed Mutagenesis of PpNRH1

Xanthosine and inosine show similar binding modes when docked into the PpNRH1 active site (Fig. 5B), with conserved interactions between the 6-oxo group and the side chains of Tyr-244 and Tyr-249 (and possibly the side chain of Lys-297) as well as between the N7 atom (protonated during catalysis) and the side chain of Tyr-241 (3.5-Å distance). Both the 2-oxo group and the N1 atom of xanthosine can form additional hydrogen bonds to the main chain carbonyl group of Asn-176. Docking experiments with uridine revealed that the 4-oxo group can interact with the hydroxyl groups of Tyr-244 and Tyr-249. The 2-oxo group points toward a cluster formed by four residues: the two imidazole rings of His-99 and His-257, the hydroxyl of Tyr-241, and the carboxyl group of Asp-29 (Fig. 5C).

To verify the results of our docking studies on substrate binding based on the PpNRH1 structure, we performed site-directed mutagenesis of Tyr-241, Tyr-244, His-245, and Tyr-249 from the mobile helix α11 and replaced them with Ala. We also mutated another residue from the α11 helix, Glu-247, whose side chain does not project into the substrate-binding site. Three other residues, Asp-250 and Asp-252, both positioned in the loop between helix α11 and strand β5, and Tyr-255, were also targeted in order to determine if more mobile regions are involved in substrate binding, as shown previously for TvNRH (Versées et al., 2002). Circular dichroism spectroscopy measurements indicate that the folding in solution of each mutant variant resembles that of WT-PpNRH1 (Supplemental Fig. S6).

The kinetic constants determined for each of the mutant variants using xanthosine and inosine as substrates are shown in Table III. The Y241A, Y244A, H245A, and Y249A mutants exhibit lower turnover rates (approximately 100-, 16-, 10-, and 22-fold lower k_{cat} values for inosine), which is consistent with their predicted role in nucleobase binding. The three mutants Y244A, H245A, and Y249A have higher K_m values (in the millimolar range) for inosine than for xanthosine, indicating a loss of interaction with the 6-oxo group of the inosine base. Because xanthosine has one more oxygen atom, the effect on K_m values is less pronounced because this additional oxygen, the 2-oxo group, could make an additional hydrogen bond to the main chain oxygen of

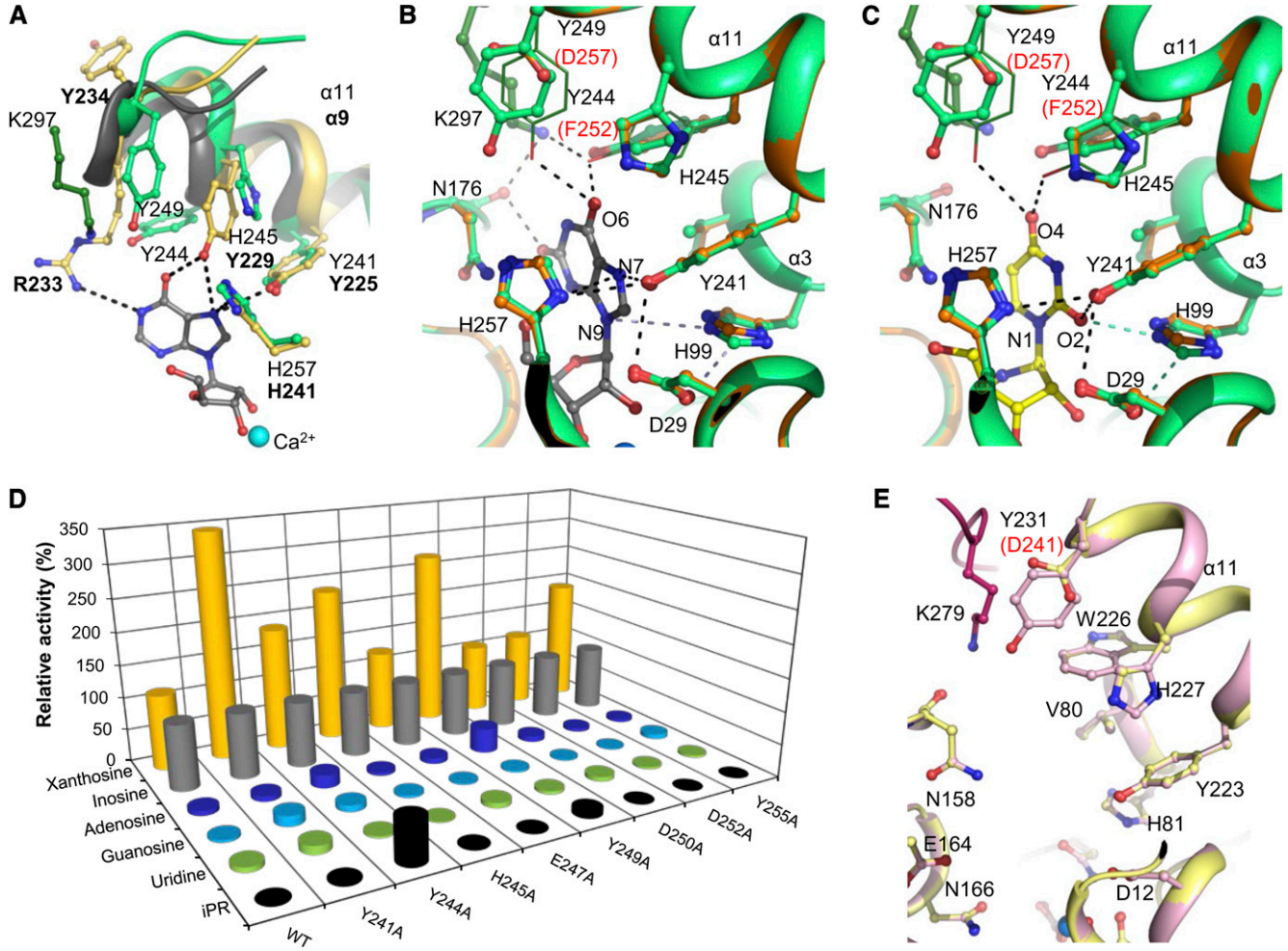

Figure 5. A, Comparison of the substrate-binding sites of PpNRH1 (green) and the IU-NRH from *C. fasciculata* (yellow; PDB 2MAS). The shift of helix α9 (in dark gray and equivalent to helix α11 in plant NRHs) that occurs upon substrate binding in the active site of YeiK is shown together with the observed position of the inosine substrate (shown in gray; PDB 3B9X). Dashed lines represent potential hydrogen bonds between the CfNRH residues and the purine base. B and C, Binding of the nucleobases of xanthosine and uridine in the active site of PpNRH1. The substrate molecules were docked into the active site of PpNRH1 (in green) using AutoDock 4.2. The rearrangements of the Tyr-249 and Tyr-244 side chains upon substrate binding are shown as lines. A model of PpNRH2 is shown in orange for comparison. Hydrogen bonds are shown as dashed lines, and those that depend on the orientation of the imidazole ring of His-99 are shown in light blue. Differences in sequence between the two NRHs are labeled in red. D, Substrate specificity of PpNRH1 proteins with six riboside substrates. Data were measured in 200 mM Tris-HCl buffer (pH 7.5) containing 400 mM KCl and 1 mM DTT and using 200 μM substrates. The activity toward inosine, as the best substrate for the wild-type enzyme, was arbitrarily taken as 100%. Using xanthosine as the substrate, a specific activity of 137 nkat mg^{-1} was measured for WT-PpNRH1, 1.2 nkat mg^{-1} for Y241A, 8.4 nkat mg^{-1} for Y244A, 14 nkat mg^{-1} for H245A, 135 nkat mg^{-1} for E247A, 6 nkat mg^{-1} for Y249A, 155 nkat mg^{-1} D250A, 66 nkat mg^{-1} for D252A, and 4.3 nkat mg^{-1} for Y255A. The D25A and H99A proteins exhibited no or negligible activity. E, Comparison of the active-site composition between ZmNRH3 (pink) and ZmNRH2b (model; light yellow). Differences in the sequences of the two NRHs are indicated by red labels.

Asn-176 (Fig. 5B). In addition, xanthosine, which is negatively charged at the studied pH, may be further stabilized by an interaction with Lys-297. In contrast, inosine exists predominantly as a neutral species at physiological pH. His-245 is fully conserved among plant NRHs, and the docking studies indicate that it does not interact with the nucleobase. However, a slight shift of helix α11, such as that observed on substrate binding in bacterial NRHs (Fig. 5A; Iovane et al., 2008), could bring its imidazole side chain into direct contact with the nucleobase, which is supported by mutagenesis results. The K_m values for the Y241A variant are higher but not as much as for the three mutants above. The residual activity of Y241A is not in favor of the catalytic acid function of this residue. However, the strongly reduced turnover rate is probably

a consequence of ineffective stabilization of the negative charge in the leaving group, leading to an increased energy barrier to reach the transition state. Because Tyr-241 is fully conserved among plant NRHs, it is most likely involved in this process and in line with similar findings on the equivalent residue in YeiK from *E. coli* and CfNRH (Iovane et al., 2008).

As expected from the structure, the E247A variant resembles the wild-type enzyme regarding activity. Both D250A and D252A also behave similarly to the wild-type enzyme, meaning that no more conformational change occurs upon substrate binding, and these residues are not in interaction with the substrate. A puzzling result was obtained with Y255A, which exhibits a 30-fold decrease in k_{cat} and a 10-fold increase in K_m values for inosine (Table III). This residue is not in direct contact with the substrate, based on docking models, but it lies in the vicinity of His-245 and His-257. Thus, it seems that the mutation has an indirect effect on catalysis by influencing the function of at least one of the two His residues.

Substrate specificity differences measured for all PpNRH1 variants with six various substrates are shown in Figure 5D. Two significant changes appear in the substrate specificity of the Y244A and Y249A proteins. First, both of the corresponding mutants have substantially higher reaction rates with adenosine (20% and 38%, respectively) compared with inosine (Fig. 5D), while WT-PpNRH1 hydrolyzes adenosine at only an 8% rate. Second, they also show higher relative rates with the cytokinin riboside iPR compared with inosine (62% and 10%, respectively), while the wild type shows only 0.1% activity. Therefore, it appears that Tyr-244 and Tyr-249 are both essential for the enzyme's activity but also have negative effects on the binding of the 6-amino group of the purine ring (in the case of adenosine) and that of the isoprenoid side chain (in the case of cytokinin ribosides).

All kinetic data correlate well with the docking experiments and highlight the essential roles of two residues, Tyr-244 and Tyr-249, in the binding of purine ribosides in PpNRH1. Notably, even though ZmNRH3 contains a Trp (Trp-226) at a position equivalent to Tyr-244 in PpNRH1, both PpNRH1 and ZmNRH3 are kinetically very similar. This suggests that the conserved Tyr-249 (Tyr-231) may be very important in determining their substrate specificity. PpNRH2, ZmNRH2a, and ZmNRH2b, which are all highly active toward uridine and xanthosine, carry an Asp residue at position 249 (Fig. 2), while all the other active-site residues remain identical (Fig. 5, B, C, and E). The Tyr replacement by an Asp is accompanied by three to five times higher K_m values for inosine and about one-half lower K_m values for uridine (Table II). This may imply that the uncharacterized PpNRH3, which also possesses an Asp, will preferentially catalyze the hydrolysis of uridine. ZmNRH1a and ZmNRH1b should behave similarly to ZmNRH3 and PpNRH1. Interestingly, AtNRH1, which exhibits higher activity toward uridine (Jung et al., 2009), also has an Asp residue at this position. We believe that the other Arabidopsis enzyme, AtNRH2, so far not kinetically characterized, should behave as ZmNRH3 and PpNRH1.

Phenotypes and Growth of *P. patens* NRH Knockout Mutants in Medium with Nucleosides as the Sole Nitrogen Source

To obtain in planta information on the function of PpNRH1, PpNRH2, and PpNRH3, we performed gene targeting and achieved a functional gene knockout by inserting a resistance cassette into each of the corresponding loci (Schaefer and Zrÿd, 1997). Three single knockout lines were selected for phenotypic analysis: d|PpNRH1#29, d|PpNRH2#56, and d|PpNRH3#7. Each of these lines satisfies all of the targeted gene knockout criteria, including the absence of detectable transcripts. When grown on full medium, all of the knockout lines had the wild-type phenotype in terms of protonema cell size and growth. When protonema suspensions were used to inoculate agar dishes, it became apparent during the first 4 weeks that all three mutant lines are delayed in bud formation (Fig. 6A). The strongest reduction in early budding is observed for d|PpNRH1#29, which exhibits only 4% of the number of buds compared with the wild type. The other mutants were less severely affected. Supplemental Figure S7 shows the significant reduction in early budding for two individual mutants for each of the PpNRH genes. The stronger phenotype of the d|PpNRH1#29 line suggests that PpNRH1 plays a more important role in cytokinin-mediated budding control in planta than do the other two PpNRHs.

We investigated the roles of each PpNRH gene product in the recycling of nucleoside-bound nitrogen by performing growth assays in which inosine, xanthosine, and adenosine were the sole nitrogen sources for nitrogen-starved tissues. The observed growth rates were compared with those achieved on a medium containing either KNO_3 or urea (Fig. 6A). All of the knockout lines perform similarly when fed with inosine and grow slightly better than on a nitrogen-free medium. However, they take on a brown color, which is indicative of nitrogen starvation in *P. patens*. Inosine has growth-inhibiting effects, which prevents the formation of gametophores. Because there are no apparent differences between the wild type and the knockout lines, we can deduce that at least two of the PpNRHs are capable of hydrolyzing inosine. The recombinant PpNRH1 and PpNRH2 proteins both hydrolyze inosine to hypoxanthine, which can be further converted to xanthine and thus act as a nitrogen source via purine degradation (Fig. 1B). Plants grown on medium containing xanthosine as the sole nitrogen source have green-colored filaments and are able to form gametophores. Again, the knockout lines have very similar phenotypes to the wild type, meaning that at least two of the three studied enzymes can convert xanthosine to xanthine and thereby enable nitrogen recycling. Both recombinant PpNRH1 and PpNRH2 hydrolyze

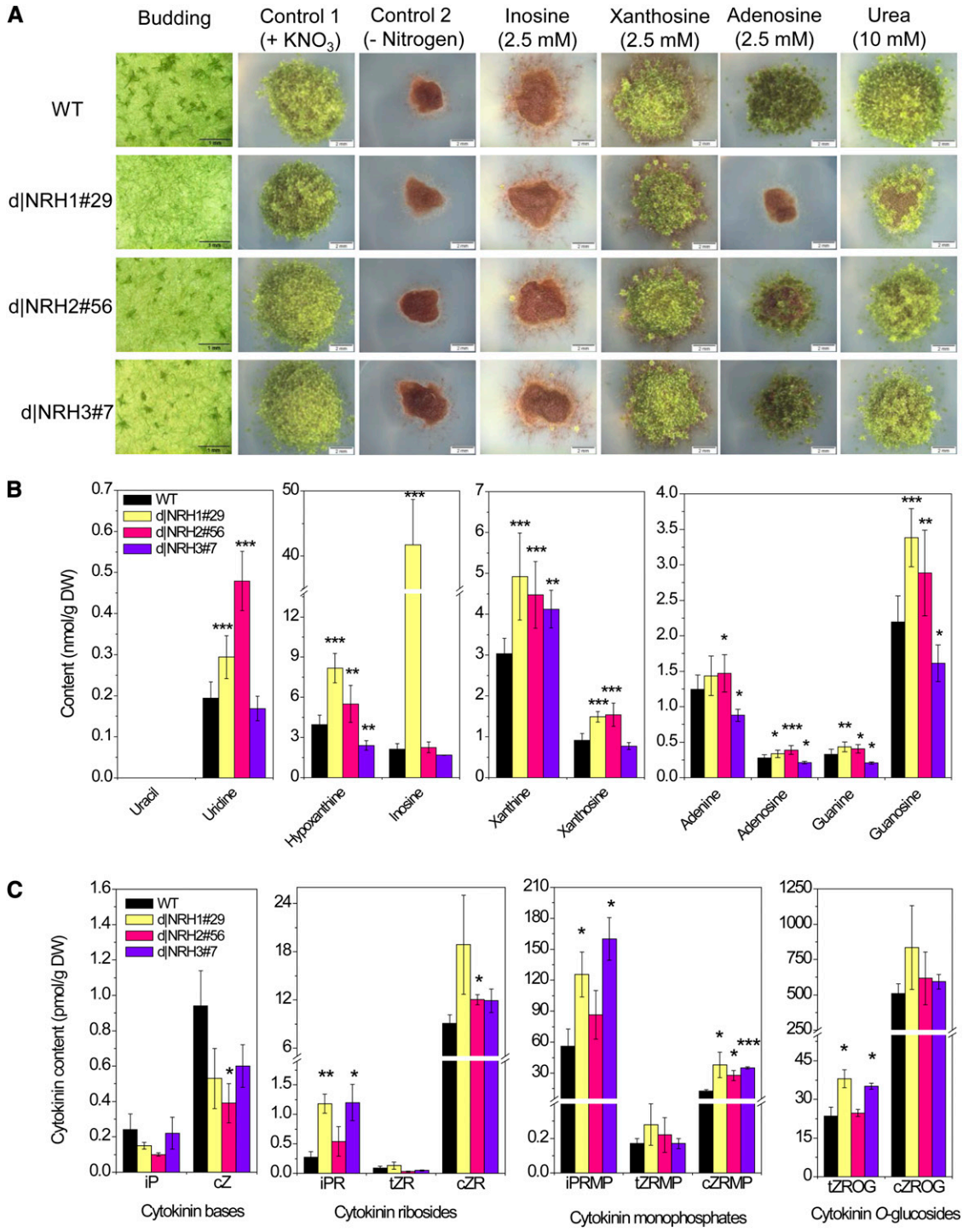

Figure 6. Phenotypic analysis of wild-type *P. patens* and three NRH knockout strains. A, Wild-type *P. patens* (WT) and the knockout strains d|PpNRH1#29, d|PpNRH2#56, and d|PpNRH3#7 were cultivated on agar medium under different conditions. The first column shows the extent of delayed budding in the mutants after 4 weeks of cultivation following aerial inoculation with a suspension of protonema cells. The second and third columns (controls 1 and 2) show cultures grown on medium containing either 10 mM KNO_3 as the sole nitrogen source or under nitrogen starvation. The remaining columns show cultures grown on medium containing 2.5 mM inosine, 2.5 mM xanthosine, or 2.5 mM adenosine as the sole nitrogen sources and an additional positive control with urea as the sole nitrogen source. Unlike the wild type, the knockout strain d|PpNRH1#29 is unable to recycle adenosine-bound nitrogen. Photographs were taken after 8 weeks. B, Levels of selected purine and pyrimidine metabolites in 21-d-old liquid-cultured protonema. The values shown represent mean values for four individual cultures per genotype; UPLC-mass spectrometry measurements were conducted in triplicate for each culture. C, Levels of selected

xanthosine (Table I). A remarkable result was obtained with medium containing adenosine as the sole nitrogen source: while the d | PpNRH2#56 and d | PpNRH3#7 knockout lines exhibited similar levels of growth to the wild type, no growth was observed for the d | PpNRH1#29 knockout line. Although recombinant PpNRH2 is weakly active toward adenosine (Table I), this finding strongly suggests that PpNRH1 is the only *P. patens* NRH that is capable of effectively recycling nitrogen from adenosine in vivo. This result clearly demonstrates that, together with xanthine dehydrogenase, NRHs play a central role in purine degradation and the recycling of nucleoside-bound nitrogen.

Changes in the Levels of Purine, Pyrimidine, and Cytokinin Metabolites in d | PpNRH Knockout Mutants

As expected from the kinetic data (Tables I and II), we observe accumulations of inosine (20-fold), uridine (1.4-fold), and xanthosine (1.5-fold) in the d | PpNRH1#29 mutant line relative to the wild type (Fig. 6B). The levels of uracil and cytidine in this mutant line are below the limit of detection. Similar accumulation is observed for uridine (2.5-fold) and xanthosine (1.6-fold) in d | PpNRH2#56 plants. Surprisingly, the level of hypoxanthine (which is produced by the hydrolysis of inosine) in the d | PpNRH1 plants is twice that in the wild type, indicating that purine metabolism is modified in this knockout. Because inosine has been found to cause growth inhibition in *P. patens* (Fig. 6A), we may assume that a harmful excess of inosine in the d | PpNRH1 mutant is eliminated by (unspecified) alternative pathways. It should be noted that Riegler et al. (2011) did not observe an accumulation of inosine over the detection limit in any of their *nrh1* and *nrh2* single and double mutants in Arabidopsis. In contrast, the AtNRH1 knockout mutant accumulates high levels of uridine in roots, which is consistent with the preferential activity of this NRH toward this substrate.

Although the xanthosine levels in the d | PpNRH1 and d | PpNRH2 plants are only slightly higher than those in the wild type, the difference is statistically significant ($P < 0.001$) and is consistent with the observation that both of the corresponding recombinant enzymes can hydrolyze this riboside. Overall, these data indicate that *P. patens* produces at least two NRHs hydrolyzing xanthosine. The levels of xanthine (a product of xanthosine hydrolysis) are increased significantly in all three knockout lines, which again suggests that they have abnormal purine metabolism due to deficiencies in NRH activity. Interestingly, the far less pronounced accumulation of xanthosine in d | PpNRH1#29 and d | PpNRH2#56 compared with that seen in the *nrh1* (*urh1*) Arabidopsis mutant (Riegler et al., 2011) suggests that bryophytes and seed plants differ in terms of xanthosine homeostasis. A comparable result (i.e. a relatively low but statistically significant increase in d | PpNRH1#29 and d | PpNRH2#56) is also found for the other purine nucleosides adenosine and guanosine. Conversely, the levels of these metabolites in the d | PpNRH3#7 plants are slightly lower than in the wild type. The finding that the levels of both the bases and the ribosides are altered indicates that their endogenous levels are regulated by both the NRHs and by enzymes that are active in other metabolic pathways, which will presumably respond to changes in the abundance of the various purine derivatives. The absence of an accumulation of uridine, inosine, and xanthosine in the d | PpNRH3#7 plants indicates that PpNRH3 probably plays a minor role in their in vivo hydrolysis, either due to low expression of the functional *PpNRH3* or because *PpNRH3* expression is specific to some developmental stage other than those examined in this work.

The first report on the functionality of AtNRH1 (Jung et al., 2009) demonstrated that recombinant enzyme is capable of hydrolyzing iPR. To date, no in planta experiments have been published showing the relevance of NRHs in cytokinin activation. The major pathway for cytokinin activation is that involving phosphoribohydrolase (LONELY GUY; Kurakawa et al., 2007), which releases cytokinin bases from the corresponding nucleotides. In mosses, N^6-(2-isopentenyl)adenine (iP) is an important cytokinin base that has significant effects on development because it induces bud formation in protonema (von Schwartzenberg et al., 2007). Our enzymatic study reveals that PpNRH1 and PpNRH2 are capable of releasing iP from the corresponding iPR, albeit at low rates (Table I). The kinetic data for ZmNRH2b and ZmNRH3 indicate that their K_m values for iPR and tZR are similar to those for other purine substrates, but their turnover rates for these substrates are much lower.

Cytokinin analyses demonstrate that the levels of endogenous iP and cis-zeatin in all three of the d | PpNRH mutant lines are slightly lower than in the wild type (the trans-zeatin levels are below the limit of detection). This is consistent with the observed hydrolysis of these cytokinin ribosides in vitro by the various PpNRH enzymes. The lower iP levels seen in our mutant lines are also consistent with their reduced levels of early bud formation. The ribosides iPR and cis-zeatin riboside as well as the ribonucleotides

Figure 6. (*Continued.*)
cytokinins in 21-d-old liquid-cultured protonema as determined by UPLC-mass spectrometry (three cultures per genotype). Asterisks indicate significant differences between the mutant lines and the wild type at *P* value thresholds of 0.05 (*), 0.01 (**), and 0.001 (***), according to Student's *t* test. Error bars indicate SD. cZ, cis-Zeatin; DW, dry weight; cZRMP, cis-zeatin riboside 5′-monophosphate; cZROG, cis-zeatin riboside-*O*-glucoside; iPRMP, isopentenyladenosine 5′-monophosphate; tZROG, trans-zeatin riboside-*O*-glucoside.

isopentenyladenosine 5′-monophosphate and cis-zeatin riboside 5′-monophosphate accumulate in all three mutant genotypes (Fig. 6C), whereas the accumulation of trans-zeatin derivatives is less pronounced. A significant accumulation of trans-zeatin riboside-*O*-glucoside is observed in d|PpNRH1#29 and d|PpNRH3#7 knockout plants. However, the levels of the cis-zeatin riboside-*O*-glucoside are only slightly elevated in d|PpNRH1#29. These observations indicate that an excess of zeatin-type ribosides is glucosylated by zeatin-*O*-glucosyltransferases. Cytokinin *O*-glucosides are generally assumed to be storage products that can be activated through hydrolysis by β-glucosidases. In summary, we can state that all three PpNRHs have an impact on cytokinin homeostasis, although we cannot rule out that some of the effects might be due to indirect or unspecific responses of the whole cytokinin homeostatic system involving other pathways in addition to NRHs.

Taken together, changes in the metabolite profiles are generally compatible with the substrate preferences determined for the recombinant PpNRHs. Unexpectedly, the increased levels of hypoxanthine, xanthine, or adenine can be possibly attributed to the activity of near pathways, including up-regulation of cytokinin oxidase/dehydrogenase, adenine deaminase, or xanthine oxidase, which might compensate the levels of these metabolites. Moreover, Jung et al. (2011) reported that the accumulation of nucleosides in the *nrh1* Arabidopsis mutant was strongly increased under conditions of prolonged darkness, when salvage pathways are more important than the biosynthetic routes. The metabolite profiling for the *P. patens* single knockout mutants was undertaken under standard conditions. In the case of ADK, another purine/cytokinin-interconverting enzyme, the expected decrease of AMP was not observed in ADK-silenced Arabidopsis plants, which was also explained by the activity of related metabolic pathways leading to AMP production (Schoor et al., 2011). NRH, ADK, and adenine phosphoribosyltransferase are similar in that the cytokinins are not their major substrates in vitro (Moffatt et al., 2000; Allen et al., 2002). Nevertheless, it was shown for the Arabidopsis ADK knockdown plants (Schoor et al., 2011) as well as for *adenine phosphoribosyltransferase1-1* mutants (Zhang et al., 2013) that the levels of endogenous cytokinins are significantly changed, revealing an impact of these enzymes on the cytokinin interconversion.

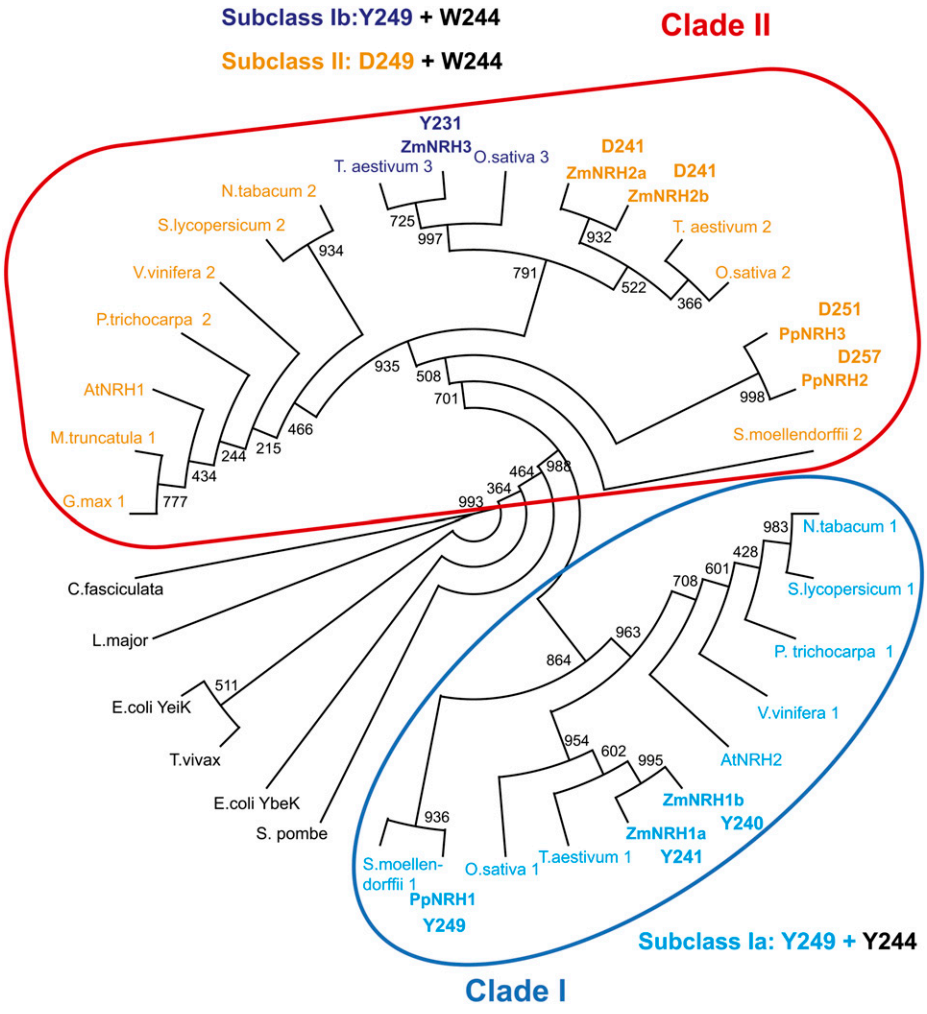

Figure 7. Cladogram of selected NRH proteins. The figure shows the clustering of plant IU-NRHs into two distinct clades (clade I and II) in the phylogenetic consensus tree. Internal labels give bootstrap frequencies for each clade. For the corresponding accession numbers, see "Materials and Methods." Subclass I (in light blue) comprises NRHs carrying a Tyr residue at position 249 (PpNRH1 numbering), which indicates preferential activity toward inosine/xanthosine. Subclass I occurs also in clade II. Subclass II (in orange) comprises NRHs carrying an Asp at position 249, which indicates preferential activity toward uridine/xanthosine.

Phylogeny of Plant IU-NRHs

Phylogenetic analysis (Fig. 7) shows clustering of plant IU-NRHs (Supplemental Fig. S8) into two clades. The outgroup comprising NRHs from *L. major*, *C. fasciculata*, *T. vivax*, *Schizosaccharomyces pombe*, and *E. coli* are, as expected, distant to the plant IU-NRHs. PpNRHs and ZmNRHs share 49% to 75% sequence identity with other plant NRHs (Supplemental Table S2). PpNRH1 is in the same branch (clade I) as ZmNRH1a and ZmNRH1b, while ZmNRH3 is in the same branch as ZmNRH2a, ZmNRH2b, PpNRH2, and PpNRH3 (clade II). It seems that early divergent land plants such as *P. patens* and *Selaginella moellendorffii* already had two NRH isoforms, which in most cases were preserved during the evolution of the seed plant line leading to two NRH isoforms, with one in each branch, in higher plants. The apparent duplication in *P. patens* resulted in *PpNRH2* and *PpNRH3* (clade II), probably due to a whole-genome duplication (Rensing et al., 2007). The Poaceae species maize, rice, and wheat display apparent diversification, leading to at least two isoforms in clade II. In the case of maize, a further diversification led to ZmNRH2a and ZmNRH2b.

There is a clear correlation between the clustering of the NRH genes and their enzymatic properties. Clade I comprises subclass 1a NRHs carrying Tyr-249 and Tyr-244 (using the PpNRH1 numbering), indicative of inosine and xanthosine preference. Clade II comprises mainly subclass II NRHs carrying an Asp at the same position (together with Trp-244), indicative of uridine/xanthosine preference. Interestingly, enzymes in clade II from the Poaceae family are also functionally diversified (Fig. 7). Although ZmNRH3 and ZmNRH2a/ZmNRH2b share 74.2% and 75.8% sequence identity (Supplemental Table S2), ZmNRH3 functionally belongs to subclass Ib (with Tyr-249 and Trp-244) and prefers the substrates inosine and xanthosine.

In the current classification, plant NRHs analyzed in this work (excluding two-domain NRHs) belong to nonspecific IU-NRHs. Our data show that assigning names of the plant IU-NRHs based on their in vitro substrate preferences can be misleading. For example, PpNRH1, which has a xanthosine/inosine preference, shows uridine as a weak substrate in vitro. However, in planta, the d|PpNRH1 line accumulates significant quantities of uridine, demonstrating that PpNRH1 is important for uridine conversion. This was the case for AtNRH1, which was initially named as uridine ribohydrolase (AtURH1; Jung et al., 2009). Plant IU-NRHs are obviously able to act on a wide range of ribosides, including cytokinin ribosides, and cannot be classified as having an exclusive preference for either purines or pyrimidines.

CONCLUSION

This work provides a comprehensive analysis of IU-NRHs from two plant species, maize and *P. patens*. It reveals the presence of several *NRH* genes per plant species, leading to the existence of at least two enzyme groups differing in substrate specificity, either preferring xanthosine/inosine (subclass I) or uridine/xanthosine (subclass II). Structural analysis combined with site-directed mutagenesis identified several residues responsible for nucleoside binding and catalysis. The single knockout mutants in *P. patens* show changes in the levels of purine, pyrimidine, and cytokinin metabolites and point out the importance of NRHs for nucleoside and cytokinin metabolism. Here, we prove the participation of plant IU-NRHs from both subclasses in cytokinin activation in vivo.

MATERIALS AND METHODS

Plant Material and Culture Conditions

The wild-type *Physcomitrella patens* (Funariaceae) strain used in this work was derived from the 'Gransden 2004' strain. Photoautotrophic growth was induced by keeping cultures under axenic conditions in growth chambers (RUMED 1602) at 25°C, illuminated with white light under a 16/8-h light/dark regime, with a flux of 50 μmol m^{-2} s^{-1}. For metabolite content analysis, tissue was cultivated in liquid medium (Wang et al., 1980) containing 0.359 mM $Ca(NO_3)_2$, 0.035 mM $FeSO_4$, 1.01 mM $MgSO_4$, 1.84 mM KH_2PO_4, and 10 mM KNO_3, to which 1 mL of Hoagland trace element solution was added (Ashton and Cove, 1977).

Cloning, Expression, and Gene Models of NRHs from *P. patens* and Maize

Total RNA for reverse transcription was isolated from *P. patens* (at the protonema stage) and from 5-d-old maize (*Zea mays* var *saccharata*) seedlings using the Plant RNA Isolation Aid solutions from Ambion. The RNA was treated twice with the TURBO DNase-free kit (Ambion). The cDNA was then synthesized using the SuperScript II reverse transcriptase (Invitrogen) and the RevertAid H Minus reverse transcriptase (Fermentas). Sequences coding for the *PpNRH1* (999 bp), *PpNRH2* (1,026 bp), and *PpNRH3* (1,017 bp) genes were amplified using gene-specific primers and the Accuprime *Pfx* polymerase (Invitrogen; Supplemental Table S3) and then cloned into a pCDFDuet His-tag vector (Novagen). In the case of PpNRH3, four splicing variants were obtained. In addition, five *NRH* coding sequences from maize were cloned (the primers used are shown in Supplemental Table S3) and submitted to GenBank. These sequences were as follows: *ZmNRH1a* (981 bp), *ZmNRH1b* (978 bp), *ZmNRH2a* (978 bp), *ZmNRH2b* (978 bp), and *ZmNRH3* open reading frame (ORF; 948 bp). The plasmids were transformed into T7 express cells (New England Biolabs). Protein expression was induced with 0.5 mM isopropyl-β-thiogalactopyranoside, after which the cultures were incubated at 20°C overnight.

Except for splicing variants of *PpNRH3_v3* and *PpNRH3_v4*, all of the analyzed *NRH* sequences consist of nine exons (Supplemental Fig. S1), with exons 2, 3, 6, and 7 all having the same length. Four variants of *PpNRH3* were identified due to alternative splicing at the 3′ ends of the fifth and eighth exons, none of which matches the current *PpNRH3* model. The eighth exon leads to a protein either with a FIAT C-terminal sequence (variants 3 and 4) or an SRLK C terminus (variants 1 and 2), in case the exon is spliced into two, meaning nine exons in total like all other NRH genes. The fifth exon, longer by 36 bp, introduces the VSLKRQKSHSRN peptide into the final protein (variants 2 and 4). Based on an alignment of plant NRH sequences, variant 1 most likely corresponds to the active form of PpNRH3. All five of the genes identified in maize also contain nine exons (Supplemental Fig. S1).

Site-Directed Mutagenesis of PpNRH1

Site-directed mutagenesis was performed on *PpNRH1* ORF in a pCDFDuet vector. The mutant H245A was prepared using two complementary primers containing the desired mutation (Supplemental Table S3). All of the other mutants were cloned using tail-to-tail-oriented phosphorylated primers, with the mutation being located at the 5′ end of one of the primers. PCR was performed using Accuprime *Pfx* polymerase (Invitrogen) in 30 cycles. The products were treated with *Dpn*I, gel purified, and ligated using the T4 DNA

ligase (Promega). The sequenced clones were transformed into T7 express competent cells (New England Biolabs). Mutant proteins were screened for the expression of the His-tagged protein by SDS-PAGE and using activity measurements.

Circular Dichroism Spectroscopy

The far-UV circular dichroism spectra of WT-PpNRH1 and its mutant variants were recorded on a J-815 spectropolarimeter (JASCO) at a concentration of 0.5 mg mL^{-1} in 20 mM Tris-HCl (pH 9.0) using a 0.1-cm quartz cell.

Phylogenetic Analysis

Amino acid alignments were performed using MUSCLE version 3.8 (Edgar, 2004). A maximum likelihood phylogeny with bootstrap analysis was performed with PhyML version 3.0 (Guindon et al., 2010) using the LG amino acid replacement matrix. *NRH* sequences from the following species were obtained from the National Center for Biotechnology Information, Phytozome, The Gene Index Project (http://compbio.dfci.harvard.edu/tgi/plant.html; Tentative Consensus accessions), or The Institute for Genomic Research (http://blast.jcvi.org/euk-blast/plantta_blast.cgi; Transcript Assembly accessions) databases: *Schizosaccharomyces pombe* (CAB91168), *Escherichia coli* YbeK (AAN79208), *E. coli* YeiK (AAA60514), *Leishmania major* (AY533501), *Crithidia fasciculata* (CFU43371), and *Trypanosoma vivax* (AF311701). Further complete plant NRH sequences were used: *P. patens* PpNRH1 (JQ649322), PpNRH2 (JX861385), and PpNRH3 (JX861386); maize ZmNRH1a (HQ825159), ZmNRH1b (HQ825160), ZmNRH2a (HQ825161), ZmNRH2b (JQ594984), and ZmNRH3 (HQ825162); Arabidopsis AtNRH1 (At2g36310) and AtNRH2 (At1g05620); soybean (*Glycine max 1*; BT097166), *Medicago truncatula 1* (XM_003625740), tobacco (*Nicotiana tabacum 1/2*; TC91311 and TC81540), rice (*Oryza sativa 1/2/3*; Os03g31170.1, Os08g44370.1, and Os09g39440.1), *Populus trichocarpa 1/2* (XM_002310348 and XM_002309011), *Selaginella moellendorffii 1/2* (XM_002974764 and XM_002984237), tomato (*Solanum lycopersicum 1/2*; AK325443 and AK322170), wheat (*Triticum aestivum 1/2/3*; TA56209_4565, TA76228_4565, and TA76014_4565), and grape (*Vitis vinifera 1/2*; XM_002280235 and XM_002283117).

Activity Measurement

Purine and pyrimidine ribosides were purchased from Sigma-Aldrich. The NRH activity was measured spectrophotometrically at 30°C according to a method described by Parkin (1996). The reaction in 200 mM Tris-HCl buffer, pH 7.5, 400 mM KCl, 1 mM dithiothreitol (DTT), and a riboside substrate was initiated by adding an appropriate amount of the enzyme (up to 50 μg for WT-PpNRH1 and 100–500 μg for the mutants). Kinetic constants were determined using the GraphPad Prism 5.0 software (GraphPad Software) by monitoring the absorption decrease of adenosine ($\Delta\varepsilon_{276} = -1.4$ mM^{-1} cm^{-1}), inosine ($\Delta\varepsilon_{280} = -0.92$ mM^{-1} cm^{-1}), uridine ($\Delta\varepsilon_{280} = -1.8$ mM^{-1} cm^{-1}), cytidine ($\Delta\varepsilon_{280} = -3.42$ mM^{-1} cm^{-1}), and thymidine ($\Delta\varepsilon_{265} = -1.7$ mM^{-1} cm^{-1}; Parkin, 1996). The differential extinction coefficients for xanthosine and guanosine were determined to be $\Delta\varepsilon_{248} = -3.7$ and -4.1 mM^{-1} cm^{-1}, respectively. Similarly, $\Delta\varepsilon_{289}$ values of -1.37 and -1.48 mM^{-1} cm^{-1} were determined for iPR and tZR, respectively.

Purification, Crystallization, and Structure Determination

All NRHs were purified on Co-Sepharose columns, and both PpNRH1 and ZmNRH3 were further purified by gel filtration chromatography on a HiLoad 26/60 Superdex 200 column using 50 mM Tris-HCl buffer (pH 8.0) and 150 mM NaCl. The purified PpNRH1 and ZmNRH3 fractions were concentrated to 30 to 35 mg mL^{-1}. Crystallization conditions for both NRHs were screened using Qiagen kits (Valencia) with a Cartesian nanodrop robot (Genomic Solutions). Crystals were obtained in hanging drops by mixing equal volumes of protein solution and a precipitant solution containing 0.1 M HEPES (pH 7.5), 100 mM sodium acetate, 10% (w/v) polyethylene glycol (PEG) 4000, and 10% ethylene glycol for PpNRH1 and containing 50 mM Tris-HCl (pH 8.0), 150 mM NaCl, and 20% (w/v) PEG 2000 monomethyl ether for ZmNRH3. Crystals were transferred to a cryoprotectant solution (the mother liquor supplemented with 25% PEG 400) and flash frozen in liquid nitrogen. Diffraction data for the PpNRH1 and ZmNRH3 crystals were collected at 100 K on the Proxima 1 beamline at the SOLEIL synchrotron at resolutions of 3.35 and 2.49 Å, respectively. Intensities were integrated using the XDS program (Kabsch, 2010; Supplemental Table S1).

The crystal structures of ZmNRH3 and PpNRH1 were determined by performing molecular replacement with Phaser (Storoni et al., 2004), using the monomer of YbeK (PDB 1YOE) and the dimer of ZmNRH3 as search models, respectively. Both models were refined with strong non-crystallographic symmetry restraints using Buster 2.10 (Bricogne et al., 2011). One translation/libration/screw-motion group was assigned for the dimer in the 2.49-Å structure and the four dimers in the lower resolution structure. Electron density maps were evaluated using COOT (Emsley and Cowtan, 2004). Refinement statistics are presented in Supplemental Table S1. No electron density was observed for residues 230 to 234 in subunit B of the ZmNRH3 structure. In subunit A, the electron density map was poorly defined for the side chains in the region comprising residues 228 to 337. Only two dimers (AB and CD) of the four were well defined in the electron density maps of the PpNRH1 structure. The dimer GH and mostly the molecule H present many disordered side chains and poor electron density maps in a few regions. Molecular graphics images were generated using PYMOL (www.pymol.org).

Substrate Docking into the Active Sites of PpNRH1 and ZmNRH3

The AutoDock suite 4.2.5.1 (Morris et al., 2009) was used for docking experiments. Both target active sites were kept rigid, while Tyr-241, Tyr-244, and Tyr-249 in PpNRH1 (Tyr-223, Trp-226, and Tyr-231 in ZmNRH3) were kept flexible. Hydrogen atoms were added and Gasteiger partial charges were computed. Calcium atom charges were added manually. Coordinates for inosine were taken from the structure of a YeiK complex (PDB 3B9X), while xanthosine and uridine were built in Avogadro 1.0.0 (http://avogadro.openmolecules.net/). The Rib moiety was constrained to maintain the C4′-endo puckered conformation, as commonly found in ribosides bound to NRHs. Docking calculations were performed using a Lamarckian genetic algorithm and a maximum of 100 conformers.

Generation of *P. patens* NRH Knockout Mutants

Functional gene knockouts of *PpNRH1*, *PpNRH2*, and *PpNRH3* were prepared using three gene-replacement vectors. The vectors were all designed using a resistance cassette flanked by 800- to 1,000-bp-long genomic fragments from the 5′ and 3′ regions of the corresponding genomic *NRH* locus. Details of the construction of the replacement vectors are provided in Supplemental Methods S1, and primer sequences are given in Supplemental Table S4. The transformation of *P. patens* protoplasts was carried out according to Schaefer et al. (1991) with minor modifications. Each transformation assay was performed using 25 μg of vector DNA. Between 15 and 20 stable moss lines were obtained after three rounds of selection using the appropriate antibiotic for each knockout construct. The haploid status of the transformants was verified, and eight to 10 transgenic lines for each mutant were arbitrarily chosen. These were then analyzed by PCR for recombination events at the corresponding loci and by reverse transcription-PCR for the absence of the transcript. Three knockout lines, d|PpNRH1#29, d|PpNRH2#56, and d|PpNRH3#7, were chosen for biochemical and phenotypic characterization.

Extraction and Determination of Purine, Pyrimidine, and Cytokinin Metabolites

P. patens wild-type and mutant lines were collected, freeze dried, and purified in triplicate (10 mg dry weight per sample). For quantification of the purine/pyrimidine bases and ribosides, the samples were homogenized, extracted in cold water with 25% ammonia (ratio, 4:1), and purified by solid-phase extraction with the addition of the stable-labeled internal standards. All samples were further purified on mixed-mode anion-exchange sorbent Oasis MAX cartridges (Waters) and analyzed using an Acquity ultra-performance liquid chromatography (UPLC) system connected to a triple quadrupole mass spectrometer (Xevo TQ MS; Waters MS Technologies). Further details are given in Supplemental Methods S1. Ultra-performance liquid chromatography-tandem mass spectrometry analysis was used to determine the cytokinin content of each sample (von Schwartzenberg et al., 2007) using a modified procedure of Novák et al. (2008).

Sequence data can be found in the GenBank/EMBL data libraries under accession numbers JQ649322 (*PpNRH1*), JX861385 (*PpNRH2*), JX861386 to JX861389 (the four splicing variants of *PpNRH3*), HQ825159 (*ZmNRH1a*), HQ825160 (*ZmNRH1b*), HQ825161 (*ZmNRH2a*), JQ594984 (*ZmNRH2b*), and HQ825162 (the *ZmNRH3* ORF). The atomic coordinates and structure factors have been deposited in the PDB under accession codes 4KPN (*PpNRH1*) and 4KPO (*ZmNRH3*).

Supplemental Data

The following materials are available in the online version of this article.

Supplemental Figure S1. *NRH* gene models for *P. patens*, maize, and Arabidopsis.

Supplemental Figure S2. Influence of pH and temperature on catalytic activity of recombinant PpNRH1.

Supplemental Figure S3. Confirmation of cytokinin riboside conversion by ZmNRH3, ZmNRH2b, and PpNRH1.

Supplemental Figure S4. Gel permeation chromatography of PpNRH1 and ZmNRH3.

Supplemental Figure S5. Structural comparison of plant NRH (ZmNRH3, this article) with NRH from *E. coli* (YeiK, PDB 3B9X).

Supplemental Figure S6. Production of PpNRH1 protein variants.

Supplemental Figure S7. Delayed bud development within 4 weeks after aerial inoculation with protonema suspension.

Supplemental Figure S8. Alignment of plant NHR sequences.

Supplemental Table S1. Data collection and refinement statistics of plant NRHs.

Supplemental Table S2. Identities of ZmNRH3 and PpNRH1 with other NRHs from maize and *P. patens* and from other species.

Supplemental Table S3. Primer pairs used for the cloning of NRHs and for the site-directed mutagenesis of PpNRH1.

Supplemental Table S4. Primers used for generation of gene replacement vectors and genetic analysis of *P. patens* knockout mutants.

Supplemental Methods S1. Generation of *P. patens* knockout mutants and quantification of ribosides.

ACKNOWLEDGMENTS

The pBZRF vector was provided by the courtesy of Fabien Nogué (Institut National de la Recherche Agronomique, Versailles). We thank Barbara Moffatt and Katja Engel (University of Waterloo) for contributions to enzyme assays in an early phase of the project, Jeanette Klein (Charité Berlin) for initial purine and pyrimidine measurements, Dr. Petr Tarkowski (University of Olomouc) for HPLC measurement, Vera Schwekendiek and Susanne Bringe (University of Hamburg) for excellent technical support, Beatriz Guimaraes for help in data collection on Proxima 1 at the SOLEIL synchrotron, Pierre Legrand (Synchrotron SOLEIL) and Gérard Bricogne (Global Phasing Ltd) for help in data processing and refinement strategy, and Andrew Thompson for help with manuscript preparation. This work benefited from the IMAGIF platform facilities (www.imagif.cnrs.fr) at the Centre de Recherche de Gif-sur-Yvette.

Received September 18, 2013; accepted October 28, 2013; published October 29, 2013.

LITERATURE CITED

Achar BS, Vaidyanathan CS (1967) Purification and properties of uridine hydrolase from mung-bean (*Phaseolus radiatus*) seedlings. Arch Biochem Biophys **119:** 356–362

Allen M, Qin W, Moreau F, Moffatt B (2002) Adenine phosphoribosyltransferase isoforms of Arabidopsis and their potential contributions to adenine and cytokinin metabolism. Physiol Plant **115:** 56–68

Ashton NW, Cove DJ (1977) The isolation and preliminary characterisation of auxotrophic and analogue resistant mutants of the moss, Physcomitrella patens. Mol Gen Genet **154:** 87–95

Bricogne G, Blanc E, Brandl M, Flensburg C, Keller P, Paciorek W, Roversi P, Sharff A, Smart OS, Vonrhein C, et al (2011) BUSTER Version 2.1.0. Global Phasing, Cambridge, UK

Campos A, Rijo-Johansen MJ, Carneiro MF, Fevereiro P (2005) Purification and characterisation of adenosine nucleosidase from *Coffea arabica* young leaves. Phytochemistry **66:** 147–151

Chen CM, Kristopeit SM (1981) Metabolism of cytokinin: deribosylation of cytokinin ribonucleoside by adenosine nucleosidase from wheat germ cells. Plant Physiol **68:** 1020–1023

Chen M, Thelen JJ (2011) Plastid uridine salvage activity is required for photoassimilate allocation and partitioning in *Arabidopsis*. Plant Cell **23:** 2991–3006

Cove D, Bezanilla M, Harries P, Quatrano R (2006) Mosses as model systems for the study of metabolism and development. Annu Rev Plant Biol **57:** 497–520

Degano M, Almo SC, Sacchettini JC, Schramm VL (1998) Trypanosomal nucleoside hydrolase: a novel mechanism from the structure with a transition-state inhibitor. Biochemistry **37:** 6277–6285

Degano M, Gopaul DN, Scapin G, Schramm VL, Sacchettini JC (1996) Three-dimensional structure of the inosine-uridine nucleoside N-ribohydrolase from *Crithidia fasciculata*. Biochemistry **35:** 5971–5981

Edgar RC (2004) MUSCLE: multiple sequence alignment with high accuracy and high throughput. Nucleic Acids Res **32:** 1792–1797

Emsley P, Cowtan K (2004) Coot: model-building tools for molecular graphics. Acta Crystallogr D Biol Crystallogr **60:** 2126–2132

Estupiñán B, Schramm VL (1994) Guanosine-inosine-preferring nucleoside N-glycohydrolase from *Crithidia fasciculata*. J Biol Chem **269:** 23068–23073

Garau G, Muzzolini L, Tornaghi P, Degano M (2010) Active site plasticity revealed from the structure of the enterobacterial N-ribohydrolase RihA bound to a competitive inhibitor. BMC Struct Biol **10:** 14

Giabbai B, Degano M (2004) Crystal structure to 1.7 a of the Escherichia coli pyrimidine nucleoside hydrolase YeiK, a novel candidate for cancer gene therapy. Structure **12:** 739–749

Gopaul DN, Meyer SL, Degano M, Sacchettini JC, Schramm VL (1996) Inosine-uridine nucleoside hydrolase from *Crithidia fasciculata*: genetic characterization, crystallization, and identification of histidine 241 as a catalytic site residue. Biochemistry **35:** 5963–5970

Guindon S, Dufayard JF, Lefort V, Anisimova M, Hordijk W, Gascuel O (2010) New algorithms and methods to estimate maximum-likelihood phylogenies: assessing the performance of PhyML 3.0. Syst Biol **59:** 307–321

Guranowski A (1982) Purine catabolism in plants: purification and some properties of inosine nucleosidase from yellow lupin (*Lupinus luteus* L.) seeds. Plant Physiol **70:** 344–349

Guranowski A, Schneider Z (1977) Purification and characterization of adenosine nucleosidase from barley leaves. Biochim Biophys Acta **482:** 145–158

Horenstein BA, Parkin DW, Estupiñán B, Schramm VL (1991) Transition-state analysis of nucleoside hydrolase from *Crithidia fasciculata*. Biochemistry **30:** 10788–10795

Houba-Hérin N, Pethe C, d'Alayer J, Laloue M (1999) Cytokinin oxidase from *Zea* mays: purification, cDNA cloning and expression in moss protoplasts. Plant J **17:** 615–626

Iovane E, Giabbai B, Muzzolini L, Matafora V, Fornili A, Minici C, Giannese F, Degano M (2008) Structural basis for substrate specificity in group I nucleoside hydrolases. Biochemistry **47:** 4418–4426

Jung B, Flörchinger M, Kunz HH, Traub M, Wartenberg R, Jeblick W, Neuhaus HE, Möhlmann T (2009) Uridine-ribohydrolase is a key regulator in the uridine degradation pathway of *Arabidopsis*. Plant Cell **21:** 876–891

Jung B, Hoffmann C, Möhlmann T (2011) Arabidopsis nucleoside hydrolases involved in intracellular and extracellular degradation of purines. Plant J **65:** 703–711

Kabsch W (2010) XDS. Acta Crystallogr D Biol Crystallogr **66:** 125–132

Kurakawa T, Ueda N, Maekawa M, Kobayashi K, Kojima M, Nagato Y, Sakakibara H, Kyozuka J (2007) Direct control of shoot meristem activity by a cytokinin-activating enzyme. Nature **445:** 652–655

Mainguet SE, Gakière B, Majira A, Pelletier S, Bringel F, Guérard F, Caboche M, Berthomé R, Renou JP (2009) Uracil salvage is necessary for early Arabidopsis development. Plant J **60:** 280–291

Massonneau A, Houba-Hérin N, Pethe C, Madzak C, Falque M, Mercy M, Kopecny D, Majira A, Rogowsky P, Laloue M (2004) Maize cytokinin oxidase genes: differential expression and cloning of two new cDNAs. J Exp Bot **55:** 2549–2557

Moffatt B, Pethe C, Laloue M (1991) Metabolism of benzyladenine is impaired in a mutant of *Arabidopsis thaliana* lacking adenine phosphoribosyltransferase activity. Plant Physiol **95:** 900–908

Moffatt B, Somerville C (1988) Positive selection for male-sterile mutants of Arabidopsis lacking adenine phosphoribosyl transferase activity. Plant Physiol **86:** 1150–1154

Moffatt BA, Stevens YY, Allen MS, Snider JD, Pereira LA, Todorova MI, Summers PS, Weretilnyk EA, Martin-McCaffrey L, Wagner C (2002) Adenosine kinase deficiency is associated with developmental abnormalities and reduced transmethylation. Plant Physiol **128:** 812–821

Moffatt BA, Wang L, Allen MS, Stevens YY, Qin W, Snider J, von Schwartzenberg K (2000) Adenosine kinase of Arabidopsis: kinetic properties and gene expression. Plant Physiol **124:** 1775–1785

Mok DW, Mok MC (2001) Cytokinin metabolism and action. Annu Rev Plant Physiol Plant Mol Biol **52:** 89–118

Morris GM, Huey R, Lindstrom W, Sanner MF, Belew RK, Goodsell DS, Olson AJ (2009) AutoDock4 and AutoDockTools4: automated docking with selective receptor flexibility. J Comput Chem **30:** 2785–2791

Muzzolini L, Versées W, Tornaghi P, Van Holsbeke E, Steyaert J, Degano M (2006) New insights into the mechanism of nucleoside hydrolases from the crystal structure of the Escherichia coli YbeK protein bound to the reaction product. Biochemistry **45:** 773–782

Novák O, Hauserová E, Amakorová P, Doležal K, Strnad M (2008) Cytokinin profiling in plant tissues using ultra-performance liquid chromatography-electrospray tandem mass spectrometry. Phytochemistry **69:** 2214–2224

Parkin DW (1996) Purine-specific nucleoside N-ribohydrolase from *Trypanosoma brucei brucei*: purification, specificity, and kinetic mechanism. J Biol Chem **271:** 21713–21719

Parkin DW, Horenstein BA, Abdulah DR, Estupiñán B, Schramm VL (1991) Nucleoside hydrolase from *Crithidia fasciculata*: metabolic role, purification, specificity, and kinetic mechanism. J Biol Chem **266:** 20658–20665

Rensing SA, Ick J, Fawcett JA, Lang D, Zimmer A, Van de Peer Y, Reski R (2007) An ancient genome duplication contributed to the abundance of metabolic genes in the moss *Physcomitrella patens*. BMC Evol Biol **7:** 130

Riegler H, Geserick C, Zrenner R (2011) *Arabidopsis thaliana* nucleosidase mutants provide new insights into nucleoside degradation. New Phytol **191:** 349–359

Riewe D, Grosman L, Fernie AR, Zauber H, Wucke C, Geigenberger P (2008) A cell wall-bound adenosine nucleosidase is involved in the salvage of extracellular ATP in *Solanum tuberosum*. Plant Cell Physiol **49:** 1572–1579

Sakakibara H (2006) Cytokinins: activity, biosynthesis, and translocation. Annu Rev Plant Biol **57:** 431–449

Schaefer D, Zryd JP, Knight CD, Cove DJ (1991) Stable transformation of the moss *Physcomitrella patens*. Mol Gen Genet **226:** 418–424

Schaefer DG, Zrÿd JP (1997) Efficient gene targeting in the moss *Physcomitrella patens*. Plant J **11:** 1195–1206

Schoor S, Farrow S, Blaschke H, Lee S, Perry G, von Schwartzenberg K, Emery N, Moffatt B (2011) Adenosine kinase contributes to cytokinin interconversion in Arabidopsis. Plant Physiol **157:** 659–672

Shi W, Schramm VL, Almo SC (1999) Nucleoside hydrolase from Leishmania major: cloning, expression, catalytic properties, transition state inhibitors, and the 2.5-Å crystal structure. J Biol Chem **274:** 21114–21120

Stasolla C, Katahira R, Thorpe TA, Ashihara H (2003) Purine and pyrimidine nucleotide metabolism in higher plants. J Plant Physiol **160:** 1271–1295

Storoni LC, McCoy AJ, Read RJ (2004) Likelihood-enhanced fast rotation functions. Acta Crystallogr D Biol Crystallogr **60:** 432–438

Szuwart M, Starzynska E, Pietrowska-Borek M, Guranowski A (2006) Calcium-stimulated guanosine-inosine nucleosidase from yellow lupin (*Lupinus luteus*). Phytochemistry **67:** 1476–1485

Versées W, Decanniere K, Pellé R, Depoorter J, Brosens E, Parkin DW, Steyaert J (2001) Structure and function of a novel purine specific nucleoside hydrolase from *Trypanosoma vivax*. J Mol Biol **307:** 1363–1379

Versées W, Decanniere K, Van Holsbeke E, Devroede N, Steyaert J (2002) Enzyme-substrate interactions in the purine-specific nucleoside hydrolase from *Trypanosoma vivax*. J Biol Chem **277:** 15938–15946

Versées W, Steyaert J (2003) Catalysis by nucleoside hydrolases. Curr Opin Struct Biol **13:** 731–738

von Schwartzenberg K (2009) Hormonal regulation of development by auxin and cytokinin in moss. Annu Plant Rev **36:** 246-281

von Schwartzenberg K, Kruse S, Reski R, Moffatt B, Laloue M (1998) Cloning and characterization of an adenosine kinase from Physcomitrella involved in cytokinin metabolism. Plant J **13:** 249–257

von Schwartzenberg K, Núñez MF, Blaschke H, Dobrev PI, Novák O, Motyka V, Strnad M (2007) Cytokinins in the bryophyte Physcomitrella patens: analyses of activity, distribution, and cytokinin oxidase/dehydrogenase overexpression reveal the role of extracellular cytokinins. Plant Physiol **145:** 786–800

Vyroubalová S, Václavíková K, Turecková V, Novák O, Smehilová M, Hluska T, Ohnoutková L, Frébort I, Galuszka P (2009) Characterization of new maize genes putatively involved in cytokinin metabolism and their expression during osmotic stress in relation to cytokinin levels. Plant Physiol **151:** 433–447

Wang TL, Cove DJ, Beutelmann P, Hartmann E (1980) Isopentenyladenine from mutants of the moss, *Physcomitrella patens*. Phytochemistry **19:** 1103–1105

Zhang X, Chen Y, Lin X, Hong X, Zhu Y, Li W, He W, An F, Guo H (2013) Adenine phosphoribosyl transferase 1 is a key enzyme catalyzing cytokinin conversion from nucleobases to nucleotides in Arabidopsis. Mol Plant **6:** 1661–1672

Zrenner R, Stitt M, Sonnewald U, Boldt R (2006) Pyrimidine and purine biosynthesis and degradation in plants. Annu Rev Plant Biol **57:** 805–836